RESEARCH ARTICLE
SOLID EARTH: TECTONOPHYSICS

Earth and Planetary Physics
10: 44–56, 2026
doi: 10.26464/epp2026011

Magnetic fabric of the late Miocene extrusive rocks of the Combia Volcanic Province: Tectonic implications for the northern Andes

Victor A. Piedrahita[1], Martin Chadima[2,3], Jackeline Ramírez[4], Alejandra Tabares[4], Maria I. Marín-Cerón[4], and JinHua Li[1,5*]

[1]Key Laboratory of Deep Petroleum Intelligent Exploration and Development, Institute of Geology and Geophysics, Chinese Academy of Sciences, Beijing 100029, China;

[2]AGICO, Purkynova 3050/99a, CZ-612 00 Brno, Czech Republic;

[3]Institute of Geology of the Czech Academy of Sciences, Rozvojová 269, CZ-165 00 Prague; 6- Lysolaje, Czech Republic;

[4]Area de territorios y ciudades, Escuela de Ciencias Aplicadas e Ingeniería, Universidad EAFIT, Medellín 050022, Colombia;

[5]College of Earth and Planetary Sciences, University of Chinese Academy Sciences, Beijing 100049, China

Key Points:

- The most significant collisional events of the Panama–Chocó Block with the South American Plate preceded the late Miocene.
- Magnetic fabrics of the extrusive rocks of the Combia Volcanic Province reveal both flow directions and deformation.
- Magnetic lineations confirm the occurrence of late Miocene volcanoes in the central axis of the Amagá Basin.

Citation: Piedrahita, V. A., Chadima, M., Ramírez, J., Tabares, A., Marín-Cerón, M. I., and Li, J. H. (2026). Magnetic fabric of the late Miocene extrusive rocks of the Combia Volcanic Province: Tectonic implications for the northern Andes. *Earth Planet. Phys.*, *10*(1), 44–56. http://doi.org/10.26464/epp2026011

Abstract: The accretion of the Panama–Chocó Block to the South American Plate partially drove the geological setting of the northern Andes. This event occurred in different collisional stages that are recorded in Oligocene–middle Miocene deformed rocks of the inter-Andean valley between the Western and Central Cordilleras of Colombia. However, uncertainty remains about the age of the latest accretionary phases of the Panama–Chocó Block. Poorly studied late Miocene volcanic rocks within the northern inter-Andean valley may provide key information to constrain the temporality of that final collision. Here, we study the deformational features of the ~12–6 Ma extrusive rocks of the Combia Volcanic Province located in the northwestern Andes (Colombia). We present anisotropy of magnetic susceptibility (AMS) data for pyroclastic and volcanic rocks within the Amagá Basin, an inter-Andean depression with Oligocene–middle Miocene sedimentary rocks that recorded NW–SE compression and NE–SW simple shear caused by the Panama–Chocó Block collision. We identified that the magnetic fabrics of the extrusive rocks of the Combia Volcanic Province reveal flow directions that indicate the occurrence of ancient volcanoes in the central axis of the Amagá Basin. Some of these fabrics do not contain any deformational features, whereas others record the same structural regime as the Oligocene–middle Miocene sedimentary rocks. We infer that variations in the intensity of the deformation promoted late Miocene local fault reactivations that, in contrast to the Oligocene–middle Miocene deformational events, did not affect the entire Amagá Basin. Age differences among the studied sections can also explain the different deformational patterns identified in the basin. Both interpretations suggest that the most significant collisional events of the Panama–Chocó Block occurred in the Oligocene–middle Miocene, whereas the formation of the Combia Volcanic Province may have either followed or coincided with the latest stages of the accretion.

Keywords: Combia Volcanic Province; Panama–Chocó Block; magnetic fabric; deformation; flow direction

1. Introduction

Neogene tectonics in the northern Andes of South America were driven by both the interaction of the Nazca, Caribbean, and South American Plates and the accretion of the allochthonous Panama–Chocó Block to northwestern South America (Cediel et al., 2003; Farris et al., 2011; Montes et al., 2012, 2015; Braszus et al., 2021). These processes caused volcanism, rock massif exhumation, and intracontinental deformation, which have been interpreted as partial evidence for an episodic collision of the Panama–Chocó Block (Farris et al., 2011; Montes et al., 2012, 2015; Piedrahita et al., 2017a; Lara et al., 2018). Despite the important climatic, biotic, and oceanographic implications of these collisional events, uncertainty remains about their temporality (Montes et al., 2015; O'Dea et al., 2016). Some geochronological, thermochronological, molecular, and fossil data have been used to suggest peak collisional activity in the Oligocene–Miocene, with the final forma-

First author: V. A. Piedrahita, u6618767@alumni.anu.edu.au
Correspondence to: J. H. Li, lijinhua@mail.iggcas.ac.cn
Received 24 AUG 2025; Accepted 23 SEP 2025.
First Published online 17 OCT 2025.

tion of a ~15–13 Ma land bridge between Central and South America (Montes et al., 2012, 2015; Bacon et al., 2015). Alternatively, other paleoclimatic and paleontological evidence indicates a contrasting scenario with earlier collisional stages that established a ~4–3 Ma isthmus (Haug and Tiedemann, 1998; O'Dea et al., 2016).

The northern Andes have key geological records that provide insights into the temporality of different tectonic events, which have been either associated with the interaction of major tectonic plates or directly related to the Panama–Chocó Block accretion (Montes et al., 2015; Piedrahita et al., 2017a, b; Lara et al., 2018; Jaramillo et al., 2019; Bernet et al., 2020). The northern Andes are characterized by the division of the Andean Belt into the Western, Central, and Eastern Cordilleras of Colombia, which are located within different geological domains that are limited by NNE–SSW major suture zones such as the Cauca and Romeral Faults (Figure 1; Taboada et al., 2000; Cediel et al., 2003; Restrepo-Moreno et al., 2009; Villagómez and Spikings, 2013). These major structures have had diverse Mesozoic–Cenozoic reactivation periods with multiple behaviors and set a fault system in the inter-Andean valley between the Western and Central Cordilleras. There, Cenozoic deformational events promoted sedimentary basin formation and subsequent sedimentary infill deformation (Ego et al., 1995; Cediel et al., 2003; Restrepo-Moreno et al., 2009; Spikings et al., 2015). The northern part of this inter-Andean valley records these geological processes within the Amagá Basin, which is located near the accretionary front of the Panama–Chocó Block (Piedrahita et al., 2017a, b, Lara et al., 2018; Escobar-Arenas et al., 2021).

The sedimentary infill of the Amagá Basin partially consists of the Oligocene–Miocene fluvial sedimentary rocks of the Amagá Formation (~28–10 Ma; Figure 2; Piedrahita et al., 2017a; Lara et al., 2018). Anisotropy of magnetic susceptibility (AMS) data of the Amagá Formation allowed identification of a NW–SE transpressive stress regime that induced syn- and postdepositional deformation resulting from different collisional stages of the Panama–Chocó Block (Piedrahita et al., 2017a). The Amagá Formation is overlaid by ~12–5 Ma lava flows and pyroclastic rocks and is intruded by ~8–7 Ma hypabyssal bodies that are related to the late Miocene Combia Volcanic Province (Figure 2; Jaramillo et al., 2019; Bernet et al., 2020; Weber et al., 2020). This magmatism was originated by the Nazca Plate subduction, and its geochemical evolution has been partially associated with variations in the subduction geometry (Jaramillo et al., 2019). Although the Combia Volcanic Province has been interpreted as a postcollisional event, it is still unknown whether significant collisional stages of the Panama–Chocó Block occurred during the eruptive phases of this volcanism or whether the final accretion itself prompted the formation of the Combia Volcanic Province (Weber et al., 2020).

Geomorphological observations have been used to suggest that the volcanoes of the Combia Volcanic Province were located in the central axis of the Amagá Basin (Figures 2 and 3; Weber et al., 2020). Cone-like landforms in this area consist of hypabyssal rocks that may represent ancient volcanic plugs (Figure 3; Calle and González, 1980; Weber et al., 2020); however, paleomagnetic and

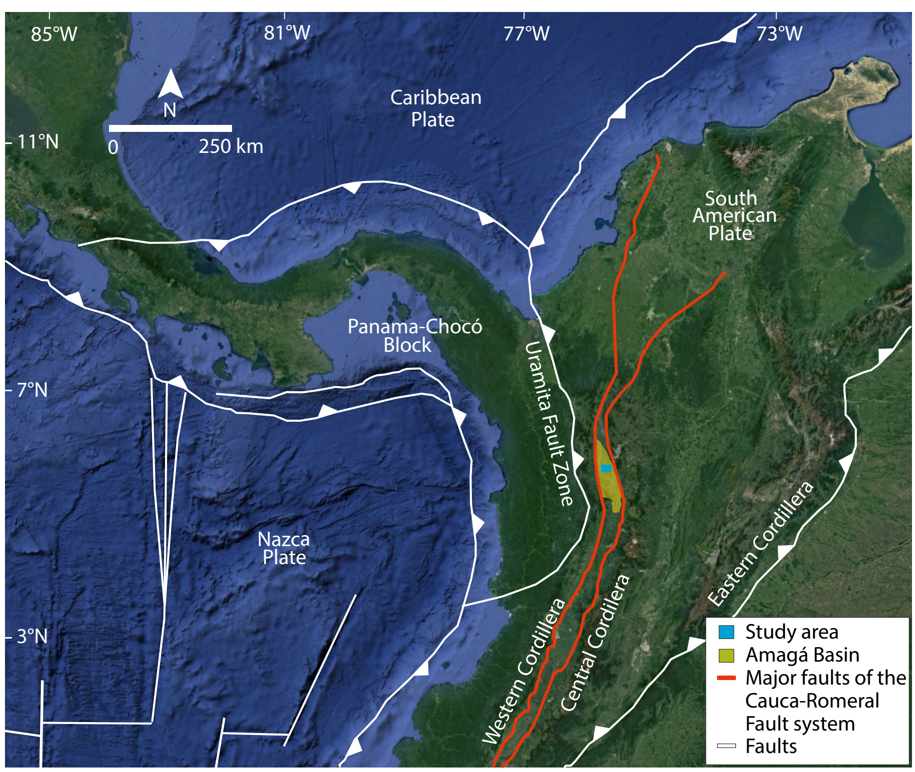

Figure 1. Geological framework of the northwestern Andes, including major tectonic plates, faults, and cordilleras. The Panama–Chocó Block, the Amagá Basin (yellow), and the study area (blue rectangle) are also indicated (Cediel et al., 2003; Villagómez and Spikings, 2013; Piedrahita et al., 2017a).

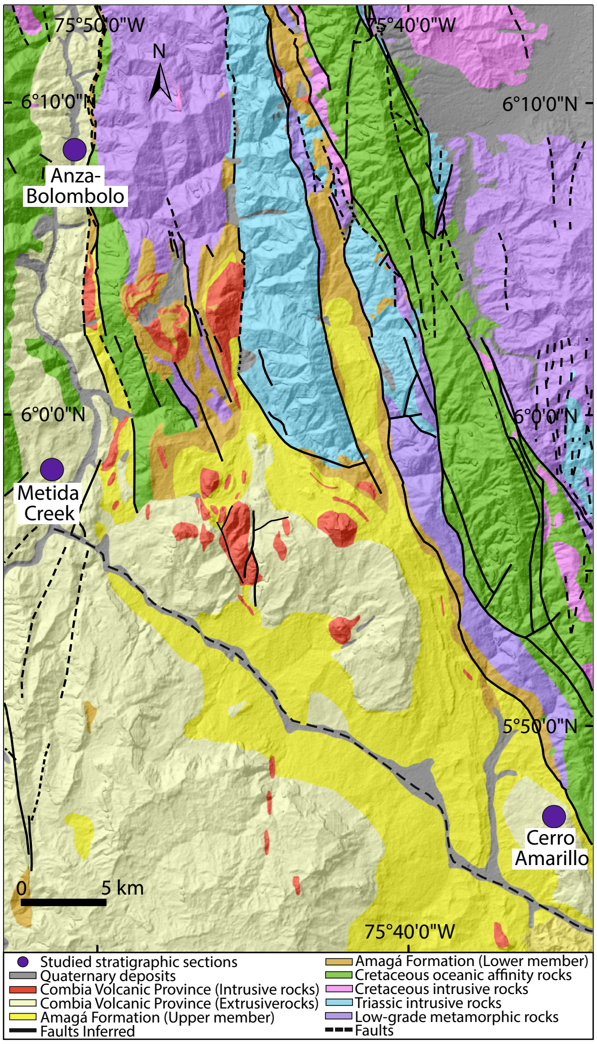

Figure 2. Geological map of the study area with the three studied stratigraphic sections of the Combia Volcanic Province (Grosse, 1926; Calle and González, 1980; Calle et al., 1980; Bernet et al., 2020).

magnetic fabric data of the hypabyssal rocks of the Combia Volcanic Province have revealed tilting and 20.2° ± 10.7° counterclockwise rotations about a vertical axis (Piedrahita et al., 2017b). These deformational features have hindered proper identification of the ancient volcanoes related to the extrusive rocks of the Combia Volcanic Province. In contrast, rock magnetic data have allowed characterization of late Miocene sinistral strike-slip kinematics (Piedrahita et al., 2017b), which are compatible with global positioning system (GPS) and geophysical data that also indicate a transpressive regime for the present-day stress field of the Amagá Basin (Cortés and Angelier, 2005; Suter et al., 2008; García-Delgado et al., 2022).

In contrast to the Amagá Formation and the hypabyssal rocks of the Combia Volcanic Province, the deformational history of the extrusive rocks of that volcanic event is still poorly studied. According to fieldwork data, these rocks appear to be tilted and folded (Bernet et al., 2020); however, a proper description of these deformational features and detailed identification of their relationship with major tectonic events remain elusive. Here, we

Figure 3. Views of hypabyssal rocks of the Combia Volcanic Province that present volcanic cone-like landforms (Weber et al., 2020).

present new AMS data on the extrusive rocks of the Combia Volcanic Province. We study magnetic fabrics in the geographic coordinate system to reconstruct the deformational history of the Combia Volcanic Province, and explore the use of the paleogeographic coordinate system to recognize ancient volcanic system locations and identify fluid mechanics (e.g., Ellwood, 1982; Incoronato et al., 1983; MacDonald and Palmer, 1990; Le Pennec et al., 1998; Pioli et al., 2008). Our new datasets provide insights into the controls of major tectonic events in the northern Andes and enhance our understanding of the Neogene interactions of the Panama–Chocó Block and the northwestern South American Plate.

2. Geological Setting

The Neogene tectonic evolution of the northern Andes is marked by the persistent Nazca Plate subduction beneath the South American Plate and the collisional stages of the allochthonous Panama–Chocó Block to the northwestern South America Plate (Cediel et al., 2003; Farris et al., 2011). The Panama–Chocó Block consists of a series of Cretaceous–Eocene volcanic and sedimentary rocks intruded by Eocene igneous bodies (Kerr et al., 1997; Buchs et al., 2011). This block collided in different episodes that began during the Oligocene–Miocene and caused orogenic pulses and intracontinental deformation (Duque-Caro, 1990; Taboada et al., 2000; Restrepo-Moreno et al., 2009; Farris et al., 2011; Villagómez and Spikings, 2013; Piedrahita et al., 2017a). Subsequent early to middle Miocene collisional stages of the Panama–Chocó Block have also been recorded by geochronological, geochemical, and structural data; however, the temporality of the last accretionary event is still under debate. Eocene detrital zircons that apparently existed only in the Panama–Chocó Block have been found in middle Miocene sedimentary rocks of the South American Plate. These data have been used to suggest a ~15–13 Ma complete Panama–Chocó Block accretion (Montes et al., 2015). Some reconstructions of terrestrial organism migrations, and Nd isotope records that reveal separated Pacific and Atlantic isotopic signatures, also support a middle–late Miocene formation of the Isthmus of Panama (Osborne et al., 2014; Bacon et al., 2015). Alternatively, other studies indicate that Eocene zircons can also be recognized in southern Colombia rock massifs, which is in line with classic paleoceanographic and paleoclimatic interpretations of a Miocene–Pliocene establishment of the Isthmus of Panama (O'Dea et al., 2016).

The northwestern margin of the South American Plate, against which the Panama–Chocó Block collided, consists of a series of Cretaceous volcanic and sedimentary rocks with oceanic affinity (Vallejo et al., 2006; Spikings et al., 2015). These rocks record the Cretaceous eastward migration of the allochthonous Caribbean Plate to its current position (Kerr et al., 1997; Villagómez et al., 2011; Hincapié-Gómez et al., 2018) and are sutured, along the Romeral Fault, to Precambrian–Jurassic metamorphic rocks located in the Central Cordillera of Colombia (Case et al., 1971; Aspden and Litherland, 1992; Ego et al., 1995; Blanco-Quintero et al., 2014; Spikings et al., 2015). West of the Romeral Fault, a similar suture, the Cauca Fault, separates different terranes with oceanic affinity rocks (Cediel et al., 2003). The Cauca and Romeral Faults constitute the Cauca–Romeral Fault System (Figure 1), which had multiple Mesozoic–Cenozoic reactivations with strike-slip motions, and undifferentiated dextral and sinistral components, that promoted basin formation and deformational events in the northern Andes (Vinasco et al., 2006; Restrepo-Moreno et al., 2009; Spikings et al., 2015; Piedrahita et al., 2017a, b).

The Oligocene–Miocene Cauca–Romeral Fault System activity promoted the formation of the Amagá Basin (Figure 1; Cediel et al., 2003; Restrepo-Moreno et al., 2009; Piedrahita et al., 2017a; Lara et al., 2018). This depression has pre-Cenozoic low-grade metamorphic rocks, Triassic and Cretaceous igneous intrusives, and Cretaceous oceanic volcanic and sedimentary rocks in its basement (Figure 2; Grosse, 1926; Calle and González, 1980; Calle et al., 1980; Piedrahita et al., 2017a; Lara et al., 2018). These rocks are covered by conglomerates, sandstones, mudstones, and coal layers that belong to the Amagá Formation, which is divided into an Oligocene–early Miocene lower member and a middle–late Miocene upper member. The Amagá Formation was deformed by Cauca–Romeral Fault System reactivations caused by the collisional stages of the Panama–Chocó Block (Piedrahita et al., 2017a). These rocks are intruded by hypabyssal rocks and overlaid by lava flows, ash beds, tuffs, and volcanic breccias with tholeiitic, calc-alkaline, and adakitic geochemical affinities that are associated with the ~12–6 Ma Combia Volcanic Province (Grosse, 1926; Calle and González, 1980; Jaramillo et al., 2019; Bernet et al., 2020; Villalba et al., 2023). This event was produced by subduction of the Nazca Plate beneath Suramerica and was preceded by a ~24–20 Ma magmatic arc that migrated from the west because of the continuous strain induced by the Panama–Chocó Block collision (Duque-Caro, 1990; Wagner et al., 2017; Jaramillo et al., 2019; Bernet et al., 2020). Petrogenetic investigations indicate that the magmatic series of the Combia Volcanic Province rocks reveal a complex tectonic scenario of variable convergence obliquity, crustal thickening, and transtensional tectonics with slightly older tholeiitic lavas than adakitic and calc-alkaline rocks (Jaramillo et al., 2019; Weber et al., 2020; Villalba et al., 2023). These rocks have been also interpreted to be strongly related to Miocene Cauca–Romeral Fault System reactivations, which promoted hypabyssal body emplacement along N–S faults and subsequent rotations over vertical and horizontal axes (Figure 2; Piedrahita et al., 2017b). Furthermore, some of these hypabyssal bodies have been interpreted to be ancient volcanic plugs because of their cone-like shapes (Figure 3; Weber et al., 2020).

3. Materials and Methods

3.1 Sampling Sites

The central part of the Amagá Basin contains extensive records of the Combia Volcanic Province (Grosse, 1926; Calle and González, 1980; Calle et al., 1980; Lara et al., 2018; Jaramillo et al., 2019). In this area, we study the Metida Creek, Anza–Bolombolo, and Cerro Amarillo sections (Figure 4; Bernet et al., 2020). The Metida Creek (5.93°N, 75.85°E) is located in the western part of the central Amagá Basin and exposes tuffs, tuff breccias, tuffaceous sandstones, lapilli tuffs, and other pyroclastic flows with NE strikes and intermediate dips to the NW. This section has zircon-fission track (ZFT) ages between 10.1 ± 2.1 Ma (2 standard errors [2SE]) and 6.7 ± 1.5 Ma and has apatite-fission track (AFT) ages that range from 15.9 ± 11.1 Ma to 8.3 ± 3.1 Ma (Figure 4a; Bernet et al., 2020). The ZFT and AFT ages of this section may not represent the specific formation of each layer, which is indicated by mismatching ages with respect to stratigraphic positions (Figure 4a). This mismatch may be a consequence of either thermal resetting by consecutive eruptive events, the presence of crystals from the basement, or both (Bernet et al., 2020). The Anza–Bolombolo section (6.15°N, 75.82°E; Figure 2) exposes subhorizontal tuffs, lapilli tuffs, pyroclastic flows, and pyroclastic breccias in the northern part of the study area. This section records eruptive events with AFT ages between 8.4 ± 3.1 Ma and. 7.9 ± 2.1 Ma (Figure 4b; Bernet et al., 2020). The Cerro Amarillo section (5.76°N, 75.58°E) contains vesicular and massive basaltic andesites in the southeastern part of the study area. This section has N–S strikes and intermediate W-oriented dips. Geochemical features of the Cerro Amarillo rocks suggest that this section is part of the tholeiitic series of the Combia Volcanic Province; hence, it is suggested to be older than the Metida Creek and Anza–Bolombolo sequences despite the lack of accurate age constraints (Figure 4c; Bernet et al., 2020; Weber et al., 2020).

3.2 Temperature-Dependent Magnetic Susceptibility Curves

To identify the magnetic susceptibility carriers of the extrusive rocks of the Combia Volcanic Province, we performed temperature-dependent magnetic susceptibility measurements in nine (9) representative samples of the three studied stratigraphic sections by using a KLY5-A Kappabridge coupled with CS-4 and CS-L temperature control units. 0.5 g of crushed samples were investigated in a quartz glass test tube, with the temperature being recorded with a platinum wire thermometer directly within the specimen powder. Complete thermomagnetic curves (from −196 °C to 700 °C and back) were obtained in three steps. First, the specimens were cooled down to the temperature of liquid nitrogen (ca. −196 °C) and then heated spontaneously to the ambient temperature (first low-temperature curve). Second, the same specimens were heated from room temperature up to 700 °C and cooled back to ambient temperature with a heating–cooling rate of ~14 °C/min (high-temperature heating–cooling curve). The high-temperature curves were acquired in a protective argon atmosphere to minimize any undesired mineral changes resulting from oxidation at elevated temperatures. Third, the specimens were again cooled down to the temperature of liquid nitrogen

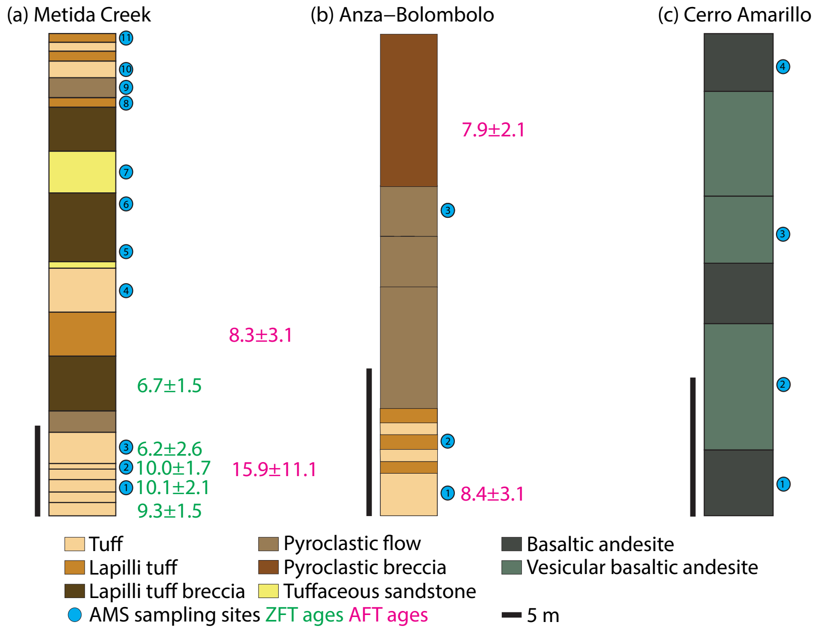

Figure 4. (a) The Metida Creek, (b) Anza–Bolombolo, and (c) Cerro Amarillo stratigraphic sections. ZFT and AFT ages are indicated (Bernet et al., 2020). AMS sampling sites with their respective labels are presented with numbers inside blue circles.

and heated spontaneously to the ambient temperature (second low-temperature curve). During all parts of the temperature experiments, magnetic susceptibility was measured approximately every 20 s.

The acquired thermomagnetic curves were processed, visualized, and analyzed using the software Cureval 8.0.2 (www.agico.com). The curves were corrected for the respective empty cryostat/furnace, and the volume-normalized bulk susceptibility (K_b) was calculated using the actual specimen mass and average density (ρ = 2.7 g cm^{-3}). For curves in which hyperbolic magnetic susceptibility decreases were visually evident according to the Curie–Weiss Law, the magnetic susceptibility was resolved into ferrimagnetic and paramagnetic components by using the hyperbola fitting technique (Hrouda, 1994; Hrouda et al., 1997).

3.3 AMS

Magnetic fabrics of the extrusive rocks of the Combia Formation are studied here with AMS data. Oriented cylindrical cores with 2.5 cm diameters were collected from 18 sampling sites in the three studied stratigraphic sections by using a gasoline-powered portable drill. These cores were cut into 2.2 cm-long samples to obtain 242 standard cylindrical specimens (>7 specimens per site). We estimated the AMS tensor of each of these specimens by using a sequence of 15 directional magnetic susceptibility measurements in a rotational design (Jelínek, 1977). These measurements were performed with a MFK1-FB Kappabridge, and our data were analyzed using the geographic and paleogeographic (tilt-corrected) coordinate systems of the Anisoft5 software (Chadima et al., 2019).

The orientation and magnitude of the three main axes of the AMS ellipsoid (K_1, K_2, and K_3) were determined using mean tensor statistics (Jelinek, 1981). The K_1 axis represents the magnetic lineation of the AMS ellipsoid, whereas K_3 characterizes the pole of the magnetic foliation plane (Jelinek, 1981). The bulk magnetic susceptibility is expressed as the mean magnetic susceptibility (K_m), which is defined as

$$K_m = \frac{(K_1 + K_2 + K_3)}{3}.$$

The shape of the AMS ellipsoid was studied through the shape parameter (T), which characterizes linear magnetic fabrics (prolate AMS ellipsoids) with negative values and planar magnetic fabrics (oblate AMS ellipsoids) with positive values. T is indicated by

$$T = \left[\frac{2(\eta_2 - \eta_3)}{(\eta_1 - \eta_3)}\right] - 1,$$

where η_1, η_2, and η_3 correspond to lnK_1, lnK_2, and lnK_3, respectively (Jelinek, 1981). The intensity of the preferred orientation of the minerals that control the magnetic fabrics is given by the anisotropy degree (P_j),

$$P_j = \exp\sqrt{\{2[(\eta_1 - \eta_m)^2 + (\eta_2 - \eta_m)^2 + (\eta_3 - \eta_m)^2]\}},$$

where η_m is defined as

$$\eta_m = \sqrt[3]{\eta_1 \cdot \eta_2 \cdot \eta_3}.$$

In addition to classic AMS scalar parameters, we estimated the angles l and f, which allow comparison of AMS directional data with mesoscopic structures. Here, l and f are defined as the angles between the bedding strike and magnetic lineation trend and between the bedding plane and the magnetic foliation plane, respectively (Chadima et al., 2006).

4. Results

4.1 Temperature-Dependent Magnetic Susceptibility Curves

The samples analyzed from the Anza–Bolombolo and Cerro Amarillo sections have relatively similar temperature-dependent magnetic susceptibility curves. High-temperature curves present clear drops at ~580 °C with irreversible cooling patterns, and low-temperature curves have continuous increases with a slight curvature at −80 °C only for the sample Cerro Amarillo 3 (Figures 5a and 5b). These features can be associated with magnetite occurrences and suggest that this mineral is the main magnetic susceptibility carrier of these samples. Some K_b decreases are also identified at ~350 °C for the sample Anza–Bolombolo 1 and at ~110 °C and ~290 °C for the sample Cerro Amarillo 1. These drops can be associated with the presence of maghemite and/or titanomagnetite (Figure 5a; Özdemir and Banerjee, 1984; Jackson and Bowles, 2014).

The samples analyzed from the Metida Creek section are characterized by lower K_b values compared with those from the Cerro Amarillo and Anza–Bolombolo sections (Figure 5c). Some heating curves of the Metida Creek samples present slight K_b drops between ~550 °C and ~580 °C, whereas the sample Metida Creek 6 has a relatively pronounced K_b decrease at ~580 °C (Figure 5c). Low-temperature curves of the Metida Creek samples do not present evidence for a Verwey transition and have hyperbolic K_b decreases that are interrupted at ~50 °C (Figure 5d). These features suggest that the magnetic susceptibility of the Metida Creek section is dominated by paramagnetic minerals, which are accompanied by smaller ferrimagnetic fractions that likely consist of magnetite or titanomagnetite.

4.2 AMS Data

4.2.1 Scalar parameters

The AMS measurements confirm observations of temperature-dependent magnetic susceptibility curves with K_m values that divide the studied sections into two groups (Figures 6a and 6b). Samples from the Cerro Amarillo and Anza–Bolombolo sections have high K_m values that can be gathered in a single group. These K_m values do not present any clear correlation with the lithological variations of the studied samples; accordingly, K_m variations across the sections are minimal. The Cerro Amarillo section has a slight K_m drop from bottom to top, whereas K_m values in the Anza–Bolombolo section remain stable (Figure 7a). A second group of samples is characterized by the comparatively lower K_m values of the Metida Creek section (Figures 6a and 6b). The K_m values of this section gradually increase from the bottom to its middle part and remain stable across the rest of the sequence (Figure 7a).

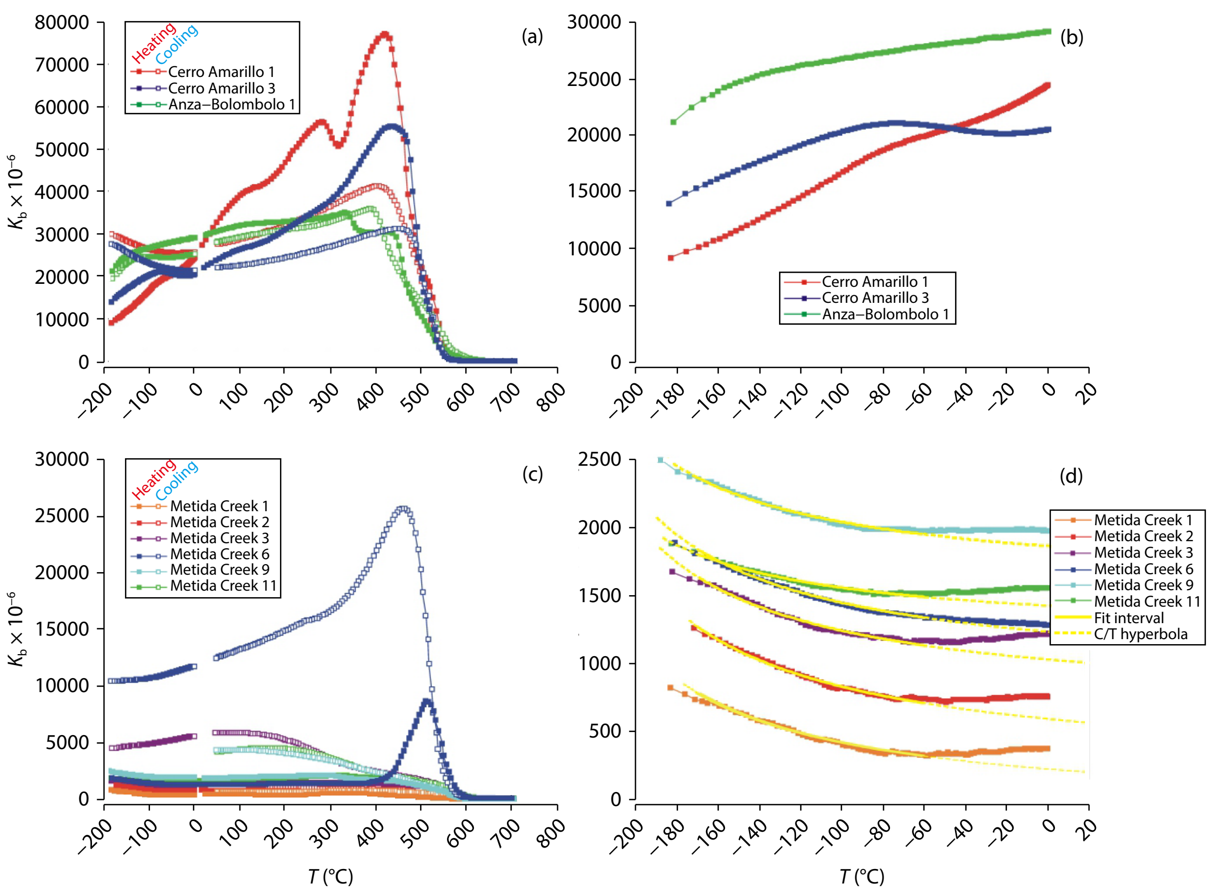

Figure 5. (a) Thermomagnetic curves of representative samples from the Cerro Amarillo and Anza–Bolombolo sections. (b) Detailed view of the low-temperature magnetic susceptibility curves of the Cerro Amarillo and Anza–Bolombolo samples. (c) Thermomagnetic curves of representative samples from the Metida Creek section. (d) Detailed view of the low-temperature magnetic susceptibility curves of the Metida Creek samples with their fitted hyperbolas.

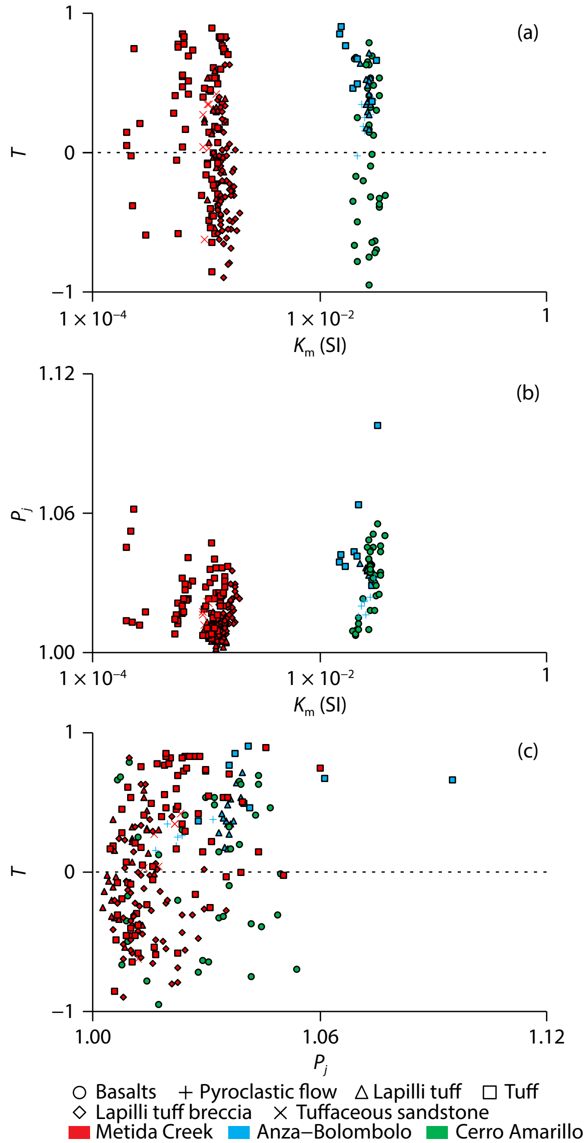

Figure 6. (a) K_m–T, (b) P_j–K_m, and (c) P_j–T plots for all analyzed specimens of the Combia Volcanic Province.

The T values of the studied samples are variable but do not have any clear correlation with the K_m. Specimens from the Cerro Amarillo section have widespread T values that set AMS ellipsoids with neutral shapes for most of the sampling sites (Figures 6a, 6b, and 7b). In contrast, samples from the Anza–Bolombolo section are characterized by positive T values related to oblate fabrics (Figures 6a, 6b, and 7b). The T values from the Metida Creek section do not follow a clear pattern that could be associated with lithology. This prevents the formation of T variability trends from bottom to top (Figures 6a, 6b, and 7b).

The P_j values of the studied samples are consistently low (<1.12) and do not have a clear relationship with K_m or T at the sample level (Figure 6c); however, some P_j trends are similar to those of T and K_m despite the low variability range of P_j. In the Cerro Amarillo section, K_m and P_j have similar fluctuations, whereas in the Anza–Bolombolo and Metida Creek sections, T and P_j follow the same trends (Figure 7c).

4.2.2 Directional parameters

The AMS directional data from the Cerro Amarillo section in the geographic coordinate system reveals magnetic lineations (K_1) with NE trends in the middle part of the sequence, and SW and NW declinations at the bottom and top of the section, respectively (Figure 8). These K_1 axes have intermediate inclinations at the bottom of the sequence and subhorizontal inclinations at its top (Figure 8). Poles to magnetic foliation (K_3) have SE–NW declinations and subhorizontal inclinations in the middle part of the section and have NE declinations and intermediate inclinations at the bottom and top (Figure 8). After tilt corrections, AMS projections in the paleogeographic coordinate system indicate changes in the magnetic lineation declinations. These then have NW trends in the middle part of the section and SW and SE declinations at the bottom and top, respectively. Alternatively, K_1 inclinations remain relatively similar to those of the geographic coordinate system (Figure 8). Tilt corrections also modify K_3, which adopts NW declinations at the bottom and top of the sequence and SE trends in the middle of the section (Figure 8). K_3 plunges also change their inclinations, which follow the same variability pattern as those of the geographic coordinate system but have higher values (Figure 8).

The Anza–Bolombolo section is characterized by almost identical K_1 and K_3 declinations and inclinations in the different coordinate systems (Figure 8). Magnetic lineations at the bottom of the section have NW declinations with subhorizontal inclinations. These values gradually change to SE trends with intermediate inclinations at the top of the sequence (Figure 8). Alternatively, K_3 axes have intermediate and subvertical inclinations characterized by SE trends at the bottom and NW directions in the middle and at the top of the section (Figure 8).

The Metida Creek section has AMS data in the geographic coordinate system with magnetic lineations that have variable inclinations and predominant NW and SW trends (Figure 8). This pattern is exclusively different at the bottom of the sequence, with NE and SE directions for K_1 (Figure 8). Alternatively, K_3 axes are characterized by NE and SE trends with variable subhorizontal and intermediate plunges (Figure 8). After tilt corrections, magnetic lineations of the Metida Creek present scattered declinations with intermediate inclinations at the bottom and top of the sequence and low inclinations in the rest of the section (Figure 8). Also in this coordinate system, K_3 axes acquire SW and NW declinations with subvertical and intermediate inclinations (Figure 8).

5. Discussion

5.1 Magnetic Fabric Origins

The extrusive rocks of the Combia Volcanic Province present contrasting AMS scalar and directional parameter patterns. These variations reflect different magnetic fabric origins, likely related to distinct depositional, rheological, or deformational processes (Tarling and Hrouda, 1993). The pyroclastic rocks of the Anza–Bolombolo section have oblate fabrics with T parameters that correlate with a nonsignificant 0.026 ± 0.022% P_j variation across the sequence (Figures 7b and 7c). The subhorizontal magnetic foliations of the Anza–Bolombolo rocks are subparallel

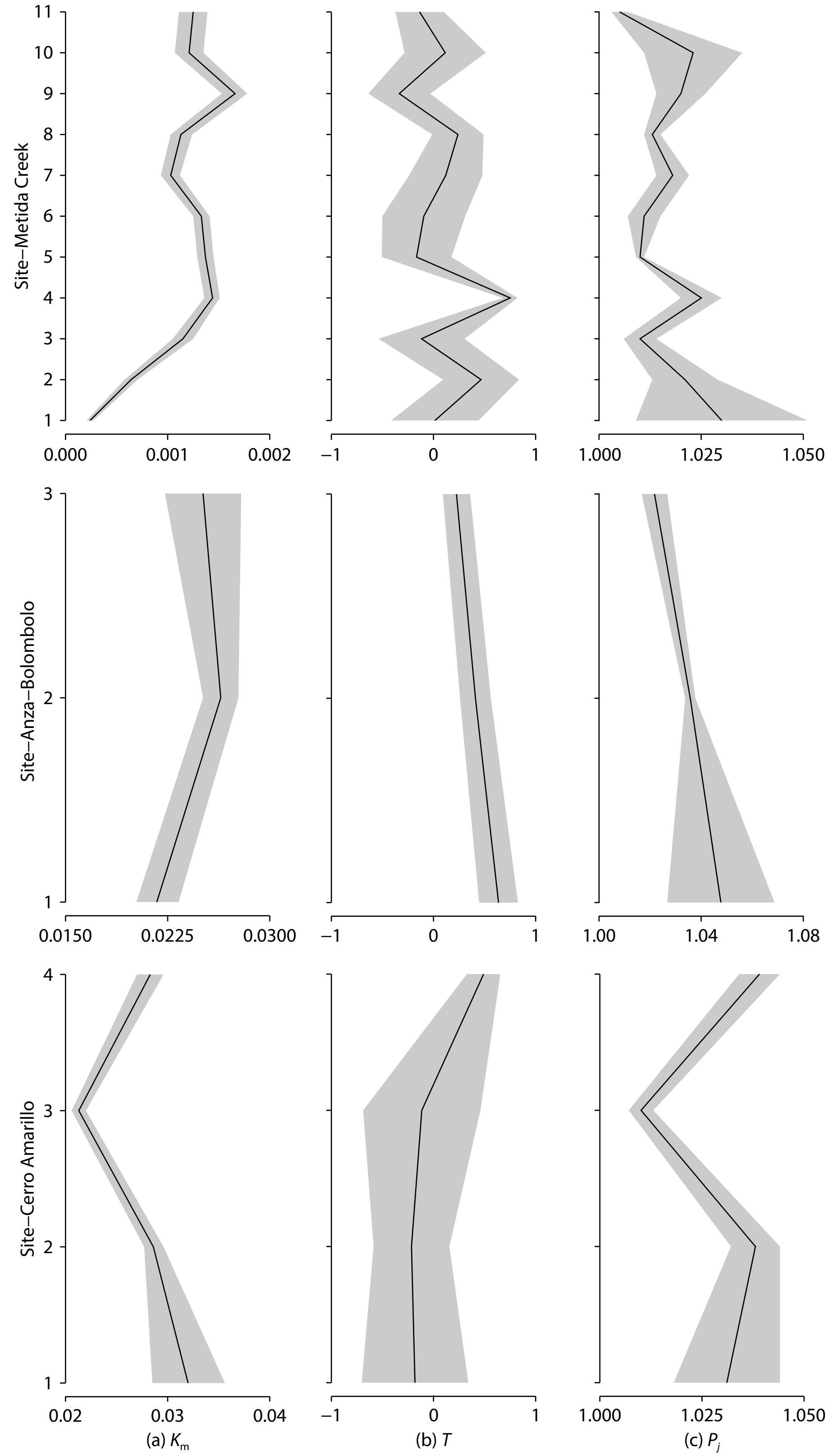

Figure 7. (a) K_m, (b) P_j, and (c) T variability across the studied stratigraphic sections. Envelopes represent the 95% confidence intervals of each site.

to the bedding plane in the geographic and paleogeographic coordinate systems (f < 40°; Figures 9 and 10), which is related to the ~3° dip of the Anza–Bolombolo strata. All these features, accompanied by subhorizontal magnetic lineations with NW–SE trends that are oblique to the bedding strike (Figures 8 and 9), suggest that the ferrimagnetic minerals that control the Anza–

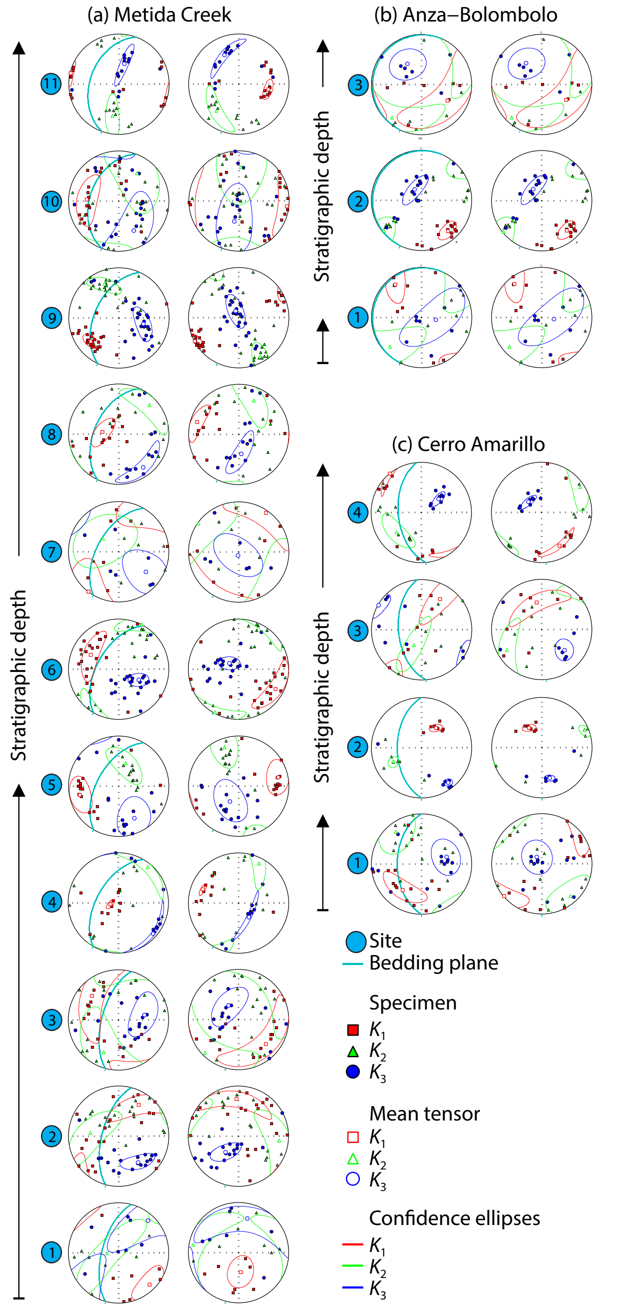

Figure 8. AMS projections of the studied sites. All data are presented in the lower hemisphere, equal-area, and geographic (left) and paleogeographic (right) coordinate systems.

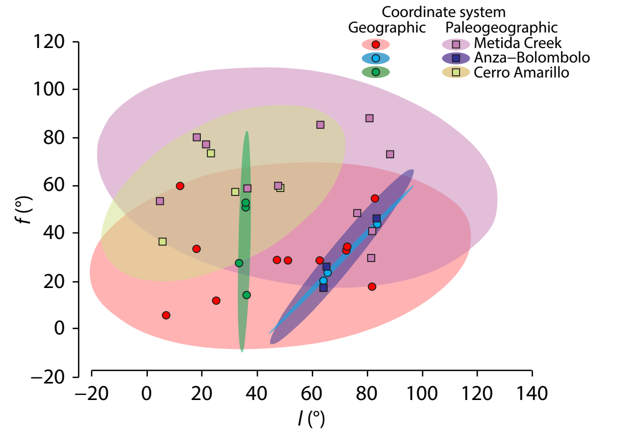

Figure 9. *I*–*f* diagram with 95% confidence ellipses estimated for each site in the geographic and paleogeographic coordinate systems.

Bolombolo AMS reveal normal magnetic fabrics without imprinted deformation (e.g., Tarling and Hrouda, 1993; Pioli et al., 2008; Fanjat et al., 2012). Therefore, we infer that the K_1 trends reflect flow directions (Figure 10), which, in the context of the location of the Anza–Bolombolo section in the NW Amagá Basin, confirm the possible occurrence of ancient volcanoes in the central axis of the inter-Andean valley (Bernet et al., 2020; Weber et al., 2020).

The AMS data on the lava flows from the Cerro Amarillo section are less consistent than those from the Anza–Bolombolo section. The correlation between mean K_m and P_j values suggests that the mineralogical assemblage may have impacts in the nature of the magnetic fabrics (Figures 7a and 7b; Tarling and Hrouda, 1993). This is confirmed by AMS projections, which reveal that magnetic fabrics can be separated into a first group with the rocks from the bottom and top of the section and into a second group with the remaining middle part of the Cerro Amarillo sequence (Figures 8 and 10). The first group develops subhorizontal lineations with SW trends in both coordinate systems. The magnetic foliation of this dataset is subhorizontal in the paleogeographic coordinate system and acquires an intermediate inclination in the geographic coordinate system (Figure 10). Alternatively, the second group of data has subvertical magnetic lineations and foliations in both coordinate systems, which indicates switched K_1 and K_3 axes with respect to the first group of data (Figure 10). This pattern suggests that one group of data records intermediate or inverse magnetic fabrics (Rochette et al., 1999; Bascou et al., 2005). These types of abnormal magnetic fabrics usually result from contrasting single-domain (SD) grain controls on magnetic fabrics (Rochette et al., 1999; Fanjat et al., 2012), which is compatible with the magnetite occurrences in the Cerro Amarillo lava flows (Figure 5). Although more rock magnetic data may be required to characterize the significance of each AMS dataset conclusively, we infer that the second group of data has abnormal fabrics because the first group has lower *f* angles (Figure 9), and the second group has tilt-corrected subvertical foliations that are not expected for AMS projections of lava flows (Figure 10; Tarling and Hrouda, 1993; Cañón-Tapia et al., 1996; Gil et al., 2002; Di Chiara et al., 2024). This interpretation suggests that the tilt-corrected SW–NE magnetic lineations of the first group of data can be associated with flow directions, which is consistent with the presence of volcanic plugs in the central axis of the Amagá Basin and the location of the Cerro Amarillo section in the eastern part of the inter-Andean valley (Figure 10). Consequently, the AMS axis deviations in the geographic coordinate system and the ~50°W dip of the Cerro Amarillo strata reveal a postemplacement deformational event (Figure 10).

The magnetic fabrics from the Metida Creek section are characterized by a T–P_j correlation that indicates that higher P_j values are

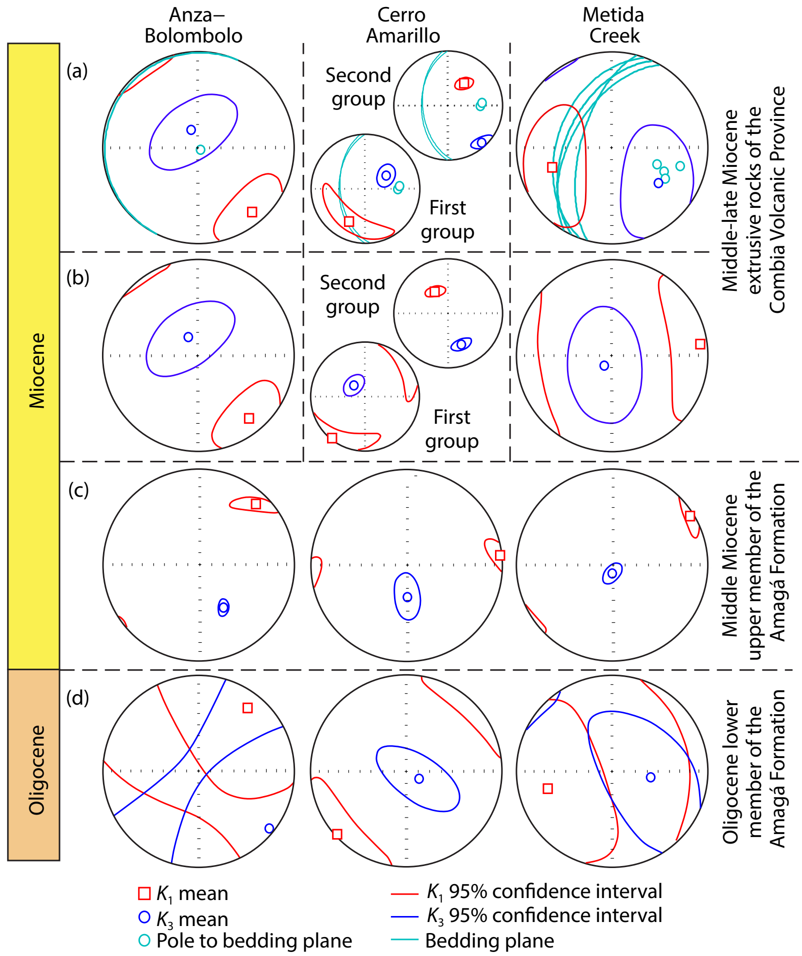

Figure 10. AMS projections for the middle–late Miocene extrusive rocks of the Combia Volcanic Province (a) in the geographic coordinate system and (b) in the paleogeographic coordinate system. AMS projections for (c) the middle Miocene upper member and (d) the Oligocene lower member of the Amagá Formation are also presented (Piedrahita et al., 2017a). Magnetic fabrics of the Amagá Formation reveal NW–SE compression with consistent NE magnetic lineations at all sites (Piedrahita et al., 2017a). All specimens of each section were compiled for these projections. Notice that the Cerro Amarillo section is divided into two groups related to normal and abnormal fabrics (see text).

related to more oblate fabrics; however, the maximum P_j variability range is only of ~3% (Figures 7b and 7c). Minimal ferrimagnetic mineral contents in the Metida Creek pyroclastic rocks, and the lack of correlation of T and P_j with K_m, suggest that abnormal fabric development by mineralogical effects may be reduced (Figures 5 and 7; Rochette et al., 1999; Fanjat et al., 2012). This assumption is partially supported by AMS projections in the paleogeographic coordinate system, which reveal that most magnetic lineations and foliations in the Metida Creek section are subhorizontal (Figure 8). Given these factors, we do not separate the Metida Creek dataset into groups for our interpretations.

Tilt-corrected AMS projections of the Metida Creek section have magnetic lineations with E–W trends that are compatible with the occurrence of ancient volcanoes in the central axis of the Amagá Basin (Figure 10; Bernet et al., 2020; Weber et al., 2020); however, 95% confidence ellipses in the *l*–*f* diagram reveal widespread data distributions that contrast with data of the undeformed rocks from the Anza–Bolombolo section (Figure 9). We infer that this may be an effect of the paramagnetic minerals that control the Metida Creek magnetic fabrics, which do not produce the well-developed AMS axes that ferrimagnetic minerals generate (Figure 5; Tarling and Hrouda, 1993). Alternatively, the large *l*–*f* 95% confidence ellipse of the Metida Creek may result from contrasting eolian–fluvial transport mechanisms, different rheological conditions between different layers, or a combination of both processes (Figure 9).

In contrast to the tilt-corrected magnetic fabrics of the Metida Creek section, AMS projections in the geographic coordinate system indicate SW-trend lineations and magnetic foliations with intermediate inclinations that coincide with the NE–SW/50°NW attitude of the strata (Figure 10). These variations reveal magnetic fabric overprinting likely related to a deformational event.

5.2 Tectonic Implications

The Amagá Basin was affected by Oligocene–Miocene NW–SE compression and NE–SW simple shear caused by different collisional stages of the Panama–Chocó Block (Piedrahita et al., 2017a). The associated transpressive stress regime of these events was identified in the Amagá Formation with NE–SW subhorizontal magnetic lineations and subvertical K_3 axes (Figure 10). Regardless of the different locations and ages recognized for the Amagá Formation, that AMS pattern was systematically recognized and related to the syn- and postdepositional deformation of this unit (Piedrahita et al., 2017a). Magnetic fabrics from the Cerro Amarillo section (first group of data) and the Metida Creek in the geographic coordinate system are reorganized with respect to the paleogeographic coordinate system. Non-tilt-corrected AMS projections of these sections have K_1 and K_3 directions similar to those of the Amagá Formation, which suggest similar deformational regimes for the late Miocene record of the Amagá Basin (Figure 10); however, these deformational features are not documented in the subhorizontal strata of the Anza–Bolombolo sequence. These contrasting patterns reveal partially different deformational conditions between the Amagá Formation and the extrusive rocks of the Combia Volcanic Province.

The identification of nondeformed extrusive rocks in the Combia Volcanic Province suggests variations in the intensity of the deformation between the Oligocene–Miocene and late Miocene record of the Amagá Basin. This finding can be explained by the activity of the Panama–Chocó Block. We infer that whereas the Oligocene–Miocene was characterized by continuous collisional events that deformed the entire Amagá Formation (Piedrahita et al., 2017a), the late Miocene Combia Volcanic Province either may have coincided with the latest stages of this accretion or may have been formed under a tectonic setting of full tectonic connection between Central and South America (Montes et al., 2015; Jaramillo et al., 2019). These conditions of contrasting tectonic activity may have promoted localized Cauca–Romeral Fault System reactivations, which allowed deformation of the Cerro Amarillo and the Metida Creek sections with the same regime that affected the Amagá Formation but did not impact other areas, such as those in which the Anza–Bolombolo section is located. Variable AMS patterns across the Combia Volcanic Province may also be related to a possible older formation of the Metida Creek and Cerro Amarillo sections compared with the Anza–Bolombolo rocks (Bernet et al., 2020; Weber et al., 2020). This scenario is also compatible with a weakened late Miocene tectonic interaction between the Panama–Chocó Block and northwestern South America (Montes et al., 2012, 2015). Although our data are limited for discussion of the age of the land connection between South and Central America, the distinct deformational features of the studied sections of the Combia Volcanic Province, and the consistent structural regime that is recorded by the Amagá Formation, reveal reduced late Miocene deformational activity in the Amagá Basin in comparison with that of the Oligocene–middle Miocene. This interpretation confirms that the most significant collisional stages of the Panama–Chocó Block preceded the eruptive phases of the Combia Volcanic Province (Farris et al., 2011; Montes et al., 2012, 2015; Bacon et al., 2015; Piedrahita et al., 2017a; Lara et al., 2018; Jaramillo et al., 2019).

6. Conclusions

The magnetic fabrics of the extrusive rocks of the Combia Volcanic Province are controlled by ferrimagnetic minerals in the Cerro Amarillo and Anza–Bolombolo sections, and mainly by paramagnetic minerals in the Metida Creek sequence. Tilt-corrected AMS data on these pyroclastic rocks and lava flows reveal flow directions with magnetic lineations, which confirm geomorphological observations and indicate the occurrence of ancient volcanoes in the central axis of the Amagá Basin (Weber et al., 2020). Magnetic fabrics in the geographic coordinate system of the Cerro Amarillo and Metida Creek sections allow the recognition of deformational events through SW lineations that are compatible with the NW–SE compression produced by the Panama–Chocó Block (Piedrahita et al., 2017a). However, that event did not affect the Anza–Bolombolo section, either because these rocks are younger or because of heterogeneous stress regimes in the Amaga Basin. Both interpretations reveal weakened late Miocene tectonic activity compared to that of the Oligocene–middle Miocene, which suggests that the most significant collisional stages of the Panama–Chocó Block with the South American Plate preceded the late Miocene Combia Volcanic Province.

Acknowledgments

This study was supported financially by the National Natural Science Foundation of China (Grants W2433104 to V.A.P. and 42225402 to J.L.), the China Postdoctoral Science Foundation (Grant 2024M753205 to V.A.P.), the Institute of Geology and Geophysics of the Chinese Academy of Sciences (International Fellowship for Postdoctoral Researchers, Grant 2025PD02 to V.A.P.), and an association between ECOS-NORD (France) and Colciencias/Icetex (Colombia) (Grant C12U01 to M.I.M.). Part of this project was developed under a junior fellowship scheme of Colciencias (Colombia) (Grant 706-2015 to V.A.P.), which also supported the undergraduate final project of A.T. We thank Juliana Mesa-Garcia, Gloria M. Sierra, and Matthias Bernet for logistical support, and two anonymous reviewers for their suggestions that improved this manuscript. V.A.P. thanks Graciela Mejía Alzate, one of the first settlers in the Combia Volcanic Province area.

References

Aspden, J. A., and Litherland, M. (1992). The geology and Mesozoic collisional history of the Cordillera Real, Ecuador. *Tectonophysics*, *205*(1-3), 187–204. https://doi.org/10.1016/00401951(92)90426-7

Bacon, C. D., Silvestro, D., Jaramillo, C., Smith, B. T., Chakrabarty, P., and Antonelli, A. (2015). Biological evidence supports an early and complex emergence of the Isthmus of Panama. *Proc. Natl. Acad. Sci. USA*, *112*(19), 6110–6115. https://doi.org/10.1073/pnas.1423853112

Bascou, J., Camps, P., and Dautria, J. M. (2005). Magnetic versus crystallographic fabrics in a basaltic lava flow. *J. Volcanol. Geotherm. Res.*, *145*(1-2), 119–135. https://doi.org/10.1016/j.jvolgeores.2005.01.007

Bernet, M., Garcia, J. M., Chauvel, C., Londoño, M. J. R., and Marín-Cerón, M. I. (2020). Thermochronological, petrographic and geochemical characteristics of the Combia Formation, Amagá basin, Colombia. *J. South Am. Earth Sci.*, *104*, 102897. https://doi.org/10.1016/j.jsames.2020.102897

Blanco-Quintero, I. F., García-Casco, A., Toro, L. M., Moreno, M., Ruiz, E. C., Vinasco, C. J., Cardona, A., Lázaro, C., and Morata, D. (2014). Late Jurassic terrane collision in the northwestern margin of Gondwana (Cajamarca complex, eastern flank of the Central Cordillera, Colombia). *Int. Geol. Rev.*, *56*(15), 1852–1872. https://doi.org/10.1080/00206814.2014.963710

Braszus, B., Goes, S., Allen, R., Rietbrock, A., Collier, J., Harmon, N., Henstock, T., Hicks, S., Rychert, C. A., … Wilson, M. (2021). Subduction history of the

Caribbean from upper-mantle seismic imaging and plate reconstruction. *Nat. Commun.*, *12*, 4211. https://doi.org/10.1038/s41467-021-24413-0

Buchs, D. M., Baumgartner, P. O., Baumgartner-Mora, C., Flores, K., and Bandini, A. N. (2011). Upper Cretaceous to Miocene tectonostratigraphy of the Azuero area (Panama) and the discontinuous accretion and subduction erosion along the Middle American margin. *Tectonophysics*, *512*(1-4), 31–46. https://doi.org/10.1016/j.tecto.2011.09.010

Calle, B., and González, H. (1980). Geología y geoquímica de la plancha 166, Jericó Escala 1:100000, Memoria explicativa. Ingeominas, Bogotá, Colombia.

Calle, B., González, H., de La Peña, D., Escorce, E., and Durango, M. (1980). Geología de la Plancha 166 Jericó, Escala 1:100000. Ingeominas, Bogotá, Colombia.

Cañón-Tapia, E., Walker, G. P. L., and Herrero-Bervera, E. (1996). The internal structure of lava flows—Insights from AMS measurements I: Near-vent a'a. *J. Volcanol. Geotherm. Res.*, *70*(1-2), 21–36. https://doi.org/10.1016/0377-0273(95)00050-X

Case, J. E., Duran S, L. G., Alfonso, L. R., and Moore, W. R. (1971). Tectonic investigations in Western Colombia and Eastern Panama. *GSA Bull.*, *82*(10), 2685–2712. https://doi.org/10.1130/0016-7606(1971)82[2685:TIIWCA]2.0.CO;2

Cediel, F., Shaw, R. P., and Cáceres, C. (2003). Tectonic assembly of the Northern Andean Block. In C. Bartolini, et al. (Eds.), *The Circum-Gulf of Mexico and the Caribbean: Hydrocarbon Habitats, Basin Formation and Plate Tectonics* (vol. 79, pp. 815–848). Tulsa, Oklahoma: AAPG. https://doi.org/10.1306/M79877C37

Chadima, M., Hrouda, F., and Melichar, R. (2006). Magnetic fabric study of the SE Rhenohercynian Zone (Bohemian Massif): Implications for dynamics of the Paleozoic accretionary wedge. *Tectonophysics*, *418*(1-2), 93–109. https://doi.org/10.1016/j.tecto.2005.12.015

Chadima, M., Hrouda, F., and Jelinek, V. (2019). Anisoft5 [Software].

Cortés, M., and Angelier, J. (2005). Current states of stress in the northern Andes as indicated by focal mechanisms of earthquakes. *Tectonophysics*, *403*(1-4), 29–58. https://doi.org/10.1016/j.tecto.2005.03.020

Di Chiara, A., Srivastava, P., Florindo, F., Gaeta, M., Marra, F., Sagnotti, L., Bonilla Alba, R., Tescione, I., Sorice, A., and Spagnuolo, L. (2024). Paleomagnetic study of the Capo di Bove lava flow, Rome, Italy. *J. Volcanol. Geotherm. Res.*, *455*, 108202. https://doi.org/10.1016/j.jvolgeores.2024.108202

Duque-Caro, H. (1990). The Choco Block in the northwestern corner of South America: Structural, tectonostratigraphic, and paleogeographic implications. *J. South Am. Earth Sci.*, *3*(1), 71–84. https://doi.org/10.1016/0895-9811(90)90019-W

Ego, F., Sébrier, M., and Yepes, H. (1995). Is the Cauca-Patia and Romeral Fault System left or right lateral?. *Geophys. Res. Lett.*, *22*(1), 33–36. https://doi.org/10.1029/94GL02837

Ellwood, B. B. (1982). Estimates of flow direction for calc-alkaline welded tuffs and paleomagnetic data reliability from anisotropy of magnetic susceptibility measurements: Central San Juan Mountains, southwest Colorado. *Earth Planet. Sci. Lett.*, *59*(2), 303–314. https://doi.org/10.1016/0012-821X(82)90133-9

Escobar-Arenas, L. C., Marín-Cerón, M. I., Restrepo-Moreno, S. A., Jaramillo, J. M., Márquez-Romero, R. E., Gamba, N. A., Barbosa-Espitia, Á., and Min, K. (2021). Low-temperature thermochronology and diagenesis of the Amagá Basin: Insights into hydrocarbon generation and its relationship with tectonothermal and hydrothermal processes. *J. South Am. Earth Sci.*, *105*, 102929. https://doi.org/10.1016/j.jsames.2020.102929

Fanjat, G., Camps, P., Shcherbakov, V., Barou, F., Sougrati, M. T., and Perrin, M. (2012). Magnetic interactions at the origin of abnormal magnetic fabrics in lava flows: A case study from Kerguelen flood basalts. *Geophysi. J. Int.*, *189*(2), 815–832. https://doi.org/10.1111/j.1365-246X.2012.05421.x

Farris, D. W., Jaramillo, C., Bayona, G., Restrepo-Moreno, S. A., Montes, C., Cardona, A., Mora, A., Speakman, R. J., Glascock, M. D., and Valencia, V. (2011). Fracturing of the Panamanian Isthmus during initial collision with South America. *Geology*, *39*(11), 1007–1010. https://doi.org/10.1130/G32237.1

García-Delgado, H., Velandia, F., Bermúdez, M. A., and Audemard, F. (2022). The present-day tectonic regimes of the Colombian Andes and the role of slab geometry in intraplate seismicity. *Int. J. Earth Sci.*, *111*(7), 2081–2099. https://doi.org/10.1007/s00531-022-02227-9

Gil, A., Lago, M., Galé, C., Pocovı, A., and Arranz, E. (2002). Magnetic fabric in folded sills and lava flows. A case study in the Permian basalts of the Anayet Massif (Pyrenean Axial Zone, Spain). *Tectonophysics, 350*(1), 1–15. https://doi.org/10.1016/S0040-1951(02)00078-1

Grosse, E. (1926). Mapa geológico de la parte occidental de la Cordillera Central entre el río Arma y Sacaojal, 1:50000. El terciario Carbonífero de Antioquia, Berlin, Germany.

Haug, G. H., and Tiedemann, R. (1998). Effect of the formation of the Isthmus of Panama on Atlantic Ocean thermohaline circulation. *Nature*, *393*(6686), 673–676. https://doi.org/10.1038/31447

Hincapié-Gómez, S., Cardona, A., Jiménez, G., Monsalve, G., Ramírez-Hoyos, L., and Bayona, G. (2018). Paleomagnetic and gravimetrical reconnaissance of Cretaceous volcanic rocks from the Western Colombian Andes: Paleogeographic connections with the Caribbean Plate. *Stud. Geophys. Geod.*, *62*(3), 485–511. https://doi.org/10.1007/s11200-016-0678-y

Hrouda, F. (1994). A technique for the measurement of thermal changes of magnetic susceptibility of weakly magnetic rocks by the CS-2 apparatus and KLY-2 Kappabridge. *Geophysi. J. Int.*, *118*(3), 604–612. https://doi.org/10.1111/j.1365-246X.1994.tb03987.x

Hrouda, F., Jelínek, V., and Zapletal, K. (1997). Refined technique for susceptibility resolution into ferromagnetic and paramagnetic components based on susceptibility temperature-variation measurement. *Geophysi. J. Int.*, *129*(3), 715–719. https://doi.org/10.1111/j.1365-246X.1997.tb04506.x

Incoronato, A., Addison, F. T., Tarling, D. H., Nardi, G., and Pescatore, T. (1983). Magnetic fabric investigations of pyroclastic deposits from Phlegrean Fields, southern Italy. *Nature*, *306*(5942), 461–463. https://doi.org/10.1038/306461a0

Jackson, M., and Bowles, J. A. (2014). Curie temperatures of titanomagnetite in ignimbrites: Effects of emplacement temperatures, cooling rates, exsolution, and cation ordering. *Geochem. Geophys. Geosyst.*, *15*(11), 4343–4368. https://doi.org/10.1002/2014GC005527

Jaramillo, J. S., Cardona, A., Monsalve, G., Valencia, V., and León, S. (2019). Petrogenesis of the late Miocene Combia volcanic complex, northwestern Colombian Andes: Tectonic implication of short term and compositionally heterogeneous arc magmatism. *Lithos, 330–331*, 194–210. https://doi.org/10.1016/j.lithos.2019.02.017

Jelínek, V. (1977). The Statistical Theory of Measuring Anisotropy of Magnetic Susceptibility of Rocks and Its Application. Geofyzika Brno, Czechoslovakia.

Jelinek, V. (1981). Characterization of the magnetic fabric of rocks. *Tectonophysics*, *79*(3-4), T63–T67. https://doi.org/10.1016/0040-1951(81)90110-4

Kerr, A. C., Marriner, G. F., Tarney, J., Nivia, A., Saunders, A. D., Thirlwall, M. F., and Sinton, C. W. (1997). Cretaceous basaltic terranes in Western Columbia: Elemental, chronological and Sr-Nd isotopic constraints on petrogenesis. *J. Petrol.*, *38*(6), 677–702. https://doi.org/10.1093/petroj/38.6.677

Lara, M., Salazar-Franco, A. M., and Silva-Tamayo, J. C. (2018). Provenance of the Cenozoic siliciclastic intramontane Amagá Formation: Implications for the early Miocene collision between Central and South America. *Sediment. Geol.*, *373*, 147–162. https://doi.org/10.1016/j.sedgeo.2018.06.003

Le Pennec, J. L., Chen, Y., Diot, H., Froger, J. L., and Gourgaud, A. (1998). Interpretation of anisotropy of magnetic susceptibility fabric of ignimbrites in terms of kinematic and sedimentological mechanisms: An Anatolian case-study. *Earth Planet. Sci. Lett.*, *157*(1-2), 105–127. https://doi.org/10.1016/S0012-821X(97)00215-X

MacDonald, W. D., and Palmer, H. C. (1990). Flow directions in ash-flow tuffs: A comparison of geological and magnetic susceptibility measurements, Tshirege member (upper Bandelier Tuff), Valles caldera, New Mexico, USA. *Bull. Volcanol.*, *53*(1), 45–59. https://doi.org/10.1007/BF00680319

Montes, C., Cardona, A., McFadden, R., Morón, S. E., Silva, C. A., Restrepo-Moreno, S., Ramírez, D. A., Hoyos, N., Wilson, J., … Flores, J. A. (2012). Evidence for Middle Eocene and younger land emergence in central

Panama: Implications for Isthmus closure. *GSA Bull.*, *124*(5-6), 780–799. https://doi.org/10.1130/B30528.1

Montes, C., Cardona, A., Jaramillo, C., Pardo, A., Silva, J. C., Valencia, V., Ayala, C., Pérez-Angel, L. C., Rodríguez-Parra, L. A., … Niño, H. (2015). Middle Miocene closure of the Central American Seaway. *Science*, *348*(6231), 226–229. https://doi.org/10.1126/science.aaa2815

O'Dea, A., Lessios, H. A., Coates, A. G., Eytan, R. I., Restrepo-Moreno, S. A., Cione, A. L., Collins, L. S., de Queiroz, A., Farris, D. W., … Jackson, J. B. C. (2016). Formation of the Isthmus of Panama. *Sci. Adv.*, *2*(8), e1600883. https://doi.org/10.1126/sciadv.1600883

Osborne, A. H., Newkirk, D. R., Groeneveld, J., Martin, E. E., Tiedemann, R., and Frank, M. (2014). The seawater neodymium and lead isotope record of the final stages of Central American Seaway closure. *Paleoceanography*, *29*(7), 715–729. https://doi.org/10.1002/2014PA002676

Özdemir, Ö., and Banerjee, S. K. (1984). High temperature stability of maghemite (γ-Fe_2O_3). *Geophys. Res. Lett.*, *11*(3), 161–164. https://doi.org/10.1029/GL011i003p00161

Piedrahita, V. A., Bernet, M., Chadima, M., Sierra, G. M., Marín-Cerón, M. I., and Toro, G. E. (2017a). Detrital zircon fission-track thermochronology and magnetic fabric of the Amagá Formation (Colombia): Intracontinental deformation and exhumation events in the northwestern Andes. *Sediment. Geol.*, *356*, 26–42. https://doi.org/10.1016/j.sedgeo.2017.05.003

Piedrahita, V. A., Molina-Garza, R. S., Sierra, G. M., and Duque-Trujillo, J. F. (2017b). Paleomagnetism and magnetic fabrics of Mio-Pliocene hypabyssal rocks of the Combia event, Colombia: Tectonic implications. *Stud. Geophys. Geod.*, *61*(4), 772–800. https://doi.org/10.1007/s11200-016-0372-0

Pioli, L., Lanza, R., Ort, M., and Rosi, M. (2008). Magnetic fabric, welding texture and strain fabric in the Nuraxi Tuff, Sardinia, Italy. *Bull. Volcanol.*, *70*(9), 1123–1137. https://doi.org/10.1007/s00445-008-0194-1

Restrepo-Moreno, S. A., Foster, D. A., Stockli, D. F., and Parra-Sánchez, L. N. (2009). Long-term erosion and exhumation of the “Altiplano Antioqueño”, Northern Andes (Colombia) from apatite (U-Th)/He thermochronology. *Earth Planet. Sci. Lett.*, *278*(1-2), 1–12. https://doi.org/10.1016/j.epsl.2008.09.037

Rochette, P., Aubourg, C., and Perrin, M. (1999). Is this magnetic fabric normal? A review and case studies in volcanic formations. *Tectonophysics*, *307*(1-2), 219–234. https://doi.org/10.1016/S0040-1951(99)00127-4

Spikings, R., Cochrane, R., Villagomez, D., Van der Lelij, R., Vallejo, C., Winkler, W., and Beate, B. (2015). The geological history of northwestern South America: From Pangaea to the early collision of the Caribbean Large Igneous Province (290–75 Ma). *Gondwana Res.*, *27*(1), 95–139. https://doi.org/10.1016/j.gr.2014.06.004

Suter, F., Sartori, M., Neuwerth, R., and Gorin, G. (2008). Structural imprints at the front of the Chocó-Panamá indenter: Field data from the North Cauca Valley Basin, Central Colombia. *Tectonophysics*, *460*(1-4), 134–157. https://doi.org/10.1016/j.tecto.2008.07.015

Taboada, A., Rivera, L. A., Fuenzalida, A., Cisternas, A., Philip, H., Bijwaard, H., Olaya, J., and Rivera, C. (2000). Geodynamics of the Northern Andes: Subductions and intracontinental deformation (Colombia). *Tectonics*, *19*(5), 787–813. https://doi.org/10.1029/2000TC900004

Tarling, D. H., and Hrouda, F. (1993). *The Magnetic Anisotropy of Rocks*. London: Chapman & Hall.

Vallejo, C., Spikings, R. A., Luzieux, L., Winkler, W., Chew, D., and Page, L. (2006). The early interaction between the Caribbean Plateau and the NW South American Plate. *Terra Nova*, *18*(4), 264–269. https://doi.org/10.1111/j.1365-3121.2006.00688.x

Villagómez, D., Spikings, R., Mora, A., Guzmán, G., Ojeda, G., Cortés, E., and Van der Lelij, R. (2011). Vertical tectonics at a continental crust–oceanic plateau plate boundary zone: Fission track thermochronology of the Sierra Nevada de Santa Marta, Colombia. *Tectonics*, *30*(4), TC4004. https://doi.org/10.1029/2010TC002835

Villagómez, D., and Spikings, R. (2013). Thermochronology and tectonics of the Central and Western Cordilleras of Colombia: Early Cretaceous-Tertiary evolution of the Northern Andes. *Lithos, 160–161*, 228–249. https://doi.org/10.1016/j.lithos.2012.12.008

Villalba, N., Murcia, H., Jerez, E., Piedrahita, D., Schonwalder-Ángel, D., Pardo-Trujillo, A., and Echeverri, S. (2023). Compositional and geothermobarometric analysis of the Upper Miocene tholeiitic volcanic products in the northern Andes at 5–6°N latitude: The Combia Volcanic Province. *Andean Geol.*, *50*(2), 181–200. https://doi.org/10.5027/andgeov50n2-3503

Vinasco, C. J., Cordani, U. G., González, H., Weber, M., and Pelaez, C. (2006). Geochronological, isotopic, and geochemical data from Permo-Triassic granitic gneisses and granitoids of the Colombian Central Andes. *J. South Am. Earth Sci.*, *21*(4), 355–371. https://doi.org/10.1016/j.jsames.2006.07.007

Wagner, L. S., Jaramillo, J. S., Ramírez-Hoyos, L. F., Monsalve, G., Cardona, A., and Becker, T. W. (2017). Transient slab flattening beneath Colombia. *Geophys. Res. Lett.*, *44*(13), 6616–6623. https://doi.org/10.1002/2017GL073981

Weber, M., Duque, J. F., Hoyos, S., Cárdenas-Rozo, A. L., Gómez, J., and Wilson, R. (2020). The Combia volcanic province: Miocene post–collisional magmatism in the northern Andes. In J. Gómez, et al. (Eds.), *The Geology of Colombia, Volume 3 Paleogene-Neogene* (vol. 37, pp. 355–394). Publicaciones Geólogicas Especiales. https://doi.org/10.32685/pub.esp.37.2019.12.